Archives of Acoustics Vol. 51, No. 3, pp. 495–506 (2026), https://doi.org/10.24423/archacoust.2026.4431

Research Paper

Low Noise Optimization of Automotive Air Conditioning Based on Response Surface Methodology

Cheng Qian(1), Dajian Wang(2), Hao Wang(2), Fushen Tang(1), Min Lin(1), Jinjin Xu(1)*

(1) *School of Energy and Power Engineering, Jiangsu University of Science and Technology*
Zhenjiang, People's Republic of China

(2) *Xiezhong International Thermal Management Systems (Jiangsu) Co., LTD.*
Nanjing, People's Republic of China

*Corresponding Author: xujinjin@just.edu.cn

Received February 4, 2026; revised May 7, 2026; accepted May 11, 2026; version of record July 28, 2026; published issue September 23, 2026.

Air conditioning is an important contributor to in-vehicle noise. In order to achieve low noise optimization, investigations were performed in a typical air conditioning unit. Computational fluid dynamics and computational aeroacoustics were combined to simulate the noise characteristics. Steady and transient simulations were conducted to identify noise sources, revealing that the dipole noise is mainly distributed on the fan blades and the volute tongue, and the fan contributes more significantly to the far-field noise. Based on the response surface methodology (RSM), three key structural parameters of the fan-volute tongue clearance, volute tongue radius, and blade outlet angle were selected as design variables, while the far-field *A*-weighted sound pressure level (SPL) was set as the response index. The final optimization parameter are: volute tongue clearance of 13.36 mm, volute tongue radius of 11.83 mm, and blade outlet angle of 110°. The far-field SPL is reduced from 61.8 dB to 55.5 dB, with a relative reduction of 10.2 %. This research validates the effectiveness and reliability of the proposed method, providing an efficient and systematic technical reference for the noise reduction design of automotive air conditioning systems.

Keywords: vehicle air conditioning, aerodynamic noise, response surface methodology, noise reduction optimization.

Copyright © 2026 The Author(s).
This work is licensed under the Creative Commons Attribution 4.0 International CC BY 4.0 (https://creativecommons.org/licenses/by/4.0/).

1. Introduction

Aerodynamic noise caused by vehicle air conditioning is identified as an important contributor to the interior noise. It could reach the interior cabin without any sound isolation and can impact customer comfort (Lee *et al.*, 2011; Singh, Mohanty, 2018; Ravichandran *et al.*, 2023). A study by the World Health Organization (WHO) points out that long-term exposure to traffic noise above 55 dB may give rise to a variety of health risks, such as cardiovascular system diseases, reduced sleep quality, and impaired mental health (Liu, Li, 2022). Therefore, how to scientifically and effectively solve the aerodynamic noise caused by vehicle air conditioning has become an important problem in the automotive industry.

To reduce internal aerodynamic noise, some studies have adjusted and optimized the structure of the air conditioning system, such as the air supply ducts and the geometric shape of the air conditioning box (Aissaoui *et al.*, 2015; Zhang *et al.*, 2021; Wu *et al.*, 2023). More studies focused on conducting targeted aerodynamic optimization on the crucial noise source, that is the centrifugal fan. A study designed five different fan models and developed a design-analysis method for testing Sirocco fan noise, whose performance and noise characteristics

were predicted within a few percent relative error (Lee, Kil, 2010). The trailing edge structures of blades were optimized. Wide serrations with a wavelength (λs) to the amplitude (2 h) ratio of $\lambda s/h = 0.6$ reduce the overall sound pressure level (SPL) by up to 11 dB (Moreau, Doolan, 2016). Research developed low-noise centrifugal fans by modifying the linear trailing edge lines of the fan blades into inclined S-shaped lines. The study confirmed the noise reductions achieved by using the inclined S-shaped trailing edges by comparing the predicted BPF noise components of the developed fans with those of the existing fan (Heo *et al.*, 2011). These researches mainly focused on a single structure optimization of the fan to achieve low noise levels, while an effective method needs to be developed that would comprehensively consider the various relevant factors affecting the fan noise.

The response surface methodology (RSM) can comprehensively take structural parameters affecting aerodynamic noise into consideration, and then obtain a noise reduction optimization solution. Compared with traditional trial-and-error optimization and single-factor analysis methods, RSM can efficiently characterize the nonlinear coupling relationship between multiple structural design variables and aerodynamic noise responses without extensive computational trials. It can construct a high-precision surrogate model with limited sample points, effectively reduce the workload of numerical simulation and parametric modeling, and significantly improve the overall optimization efficiency. The RSM has been widely applied in the research of aerodynamic noise reduction optimization. A study combined the RSM with the partial differential equation (PDE) method to investigate the aerodynamic design problem of flying wings (Sevant *et al.*, 2000). Another study established an optimization function between optimization variables and multi-objective performance by integrating the RSM and the entropy weight method (Zhang *et al.*, 2017). The RSM is also used for structural noise reduction optimization of fans. Researchers adopted the RSM for the rational optimization of fan structural parameters, achieving the optimal control of aerodynamic noise levels (Yang *et al.*, 2013). Others designed a Box–Behnken test based on the RSM, and established the relationship between fan performance and boundary parameters using a quadratic regression surrogate model. A comprehensive evaluation function for fan performance is proposed in the research, therefore obtaining the optimal layout strategy for the dual-fan system (Guo *et al.*, 2022).

However, the studies mostly take the SPL of the fan itself as the response index. Considering the practical application of fan in automobile air conditioning system, noise characteristics and fan noise reduction optimization need to be explored and discussed in the whole automobile air conditioning box. The far-field A-weighted SPL of the vehicle air conditioning cabinet was taken as the response index in the study and the optimal fan structural parameter was determined for reducing the noise.

2. Methodology

2.1. Aeroacoustic theoretical equations

The basic aeroacoustic equations are the theoretical foundation for solving aerodynamic noise problems. British mathematician James Lighthill reorganized and transformed the Navier–Stokes (N-S) equations. He proposed the Lighthill equation and the eighth-power law. The specific expressions of the Lighthill equation are shown in Eq. (1) and Eq. (2), and the expression of the eighth-power law is given in Eq. (3):

$$\frac{\partial^2 \rho'}{\partial t^2} - c_0^2 \nabla^2 \rho' = \frac{\partial^2 T_{ij}}{\partial x_i \partial x_j}, \tag{1}$$

$$T_{ij} = \rho u_i u_j - \sigma_{ij} + \left[(p - p_0) - c_0^2 (\rho - \rho_0)\right] \delta_{ij}, \tag{2}$$

where ρ' is the disturbance quantity of fluid density, c_0 is the speed of sound, T_{ij} is the Lighthill stress tensor, which represents the turbulent stress inside the fluid, p_0 is the ambient pressure, δ_{ij} is the Kronecker delta function;

$$P \propto \rho_0 U^8 a_0^{-5} L^2, \tag{3}$$

where P is the radiated sound power of turbulent noise, ρ_0 is the fluid density, U is the characteristic velocity of the flow (e.g., turbulent velocity), L is the characteristic length scale.

Newby Curle, a British mathematician, proposed the Curle equation based on the Lighthill theory, further improving the theoretical system of aeroacoustics. The specific expression of the Curle equation is as follows:

$$\rho'(\mathbf{x},t) = \frac{1}{4\pi c_0^2}\int_V \frac{\partial^2 T_{ij}}{\partial y_i \partial y_j}\frac{1}{|\mathbf{x}-\mathbf{y}|}\,\mathrm{d}^3\mathbf{y} + \frac{1}{4\pi c_0^2}\int_S \left(\frac{\partial p}{\partial n}\frac{1}{|\mathbf{x}-\mathbf{y}|} - \frac{\rho_0 v_n}{|\mathbf{x}-\mathbf{y}|^2}\right)\mathrm{d}S(\mathbf{y}), \tag{4}$$

where $\rho'(\mathbf{x},t)$ is the density fluctuation in the sound field, c_0 is the speed of sound, T_{ij} is the Lighthill stress tensor, p is the pressure on the solid boundary, v_n is the normal velocity on the solid boundary, S is the solid boundary surface, V is the fluid volume.

Ffowcs Williams and Hawkings proposed the Ffowcs Williams–Hawkings (FW-H) equation. This equation expands the application scope of the aeroacoustics theory. The mathematical form of the FW-H equation is shown in Eq. (5):

$$\frac{1}{c_0^2}\frac{\partial^2 p}{\partial t^2} - \nabla^2 p = \frac{\partial^2}{\partial x_i \partial x_j}T_{ij}H(f) - \frac{\partial}{\partial x_i}[p_{ij}n_i + \rho u_i(u_n - v_n)]\delta(f) - \frac{\partial}{\partial t}[\rho_0 v_n + \rho(u_n - v_n)]\delta(f), \tag{5}$$

$$H(f) = \begin{cases} 1 & f > 0, \\ 0 & f < 0, \end{cases} \tag{6}$$

$$\delta(f) = \frac{\partial H}{\partial f} = \begin{cases} 1 & f = 0, \\ 0 & f \neq 0, \end{cases} \tag{7}$$

where c_0 is the far-field speed of sound, t is the reception time, p is the sound pressure, p_{ij} is the pressure stress tensor, n_j is the unit normal vector pointing outward to the external region, u_i is the fluid velocity component in the i-th direction, u_n is the normal fluid velocity of the integral surface, v_n is the normal velocity of the integral surface, ρ and ρ_0 are the perturbed density and the initial density, $\delta(f)$ is the Dirac function, which is used to describe the source term on the boundary, $H(f)$ is the Heaviside function, which is used to distinguish between the fluid region and the solid region.

2.2. Physical model

The automotive air conditioning system consists of several key components, including the internal and external circulation air inlets, filter, fan, fan volute, evaporator, heater, and air control valves. By adjusting the air valve, different air conditioning blowing and working modes can be switched according to actual requirements. The study took the full-cool face blowing mode as an example to analyze the aerodynamic noise characteristics and noise propagation mechanisms. A simplified simulation model was developed based on the physical structure of the air conditioning unit. Minor components and non-critical structures were reasonably simplified, and the filter and evaporator were treated as porous media. The simplified air conditioning system model is shown in Fig. 1.

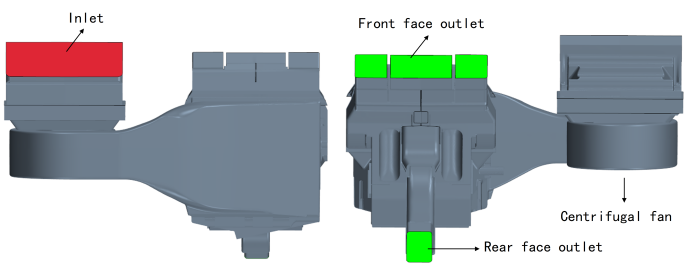

Fig. 1. Simplified model diagram of the air conditioning system.

2.3. Mesh generation and grid-independence verification

Considering that the simulation model has a complex structure, with large curvature changes and rich detailed features in local areas, triangular meshes were used for surface meshing, with the mesh size controlled within the

range of 1 mm to 4 mm. Local densification was applied to the air inlets, air outlets, fan blades, porous media regions, pipeline corners, and areas with significant changes in structural parameters. Finally, the number of surface meshes reached 1.15 million, as shown in Fig. 2.

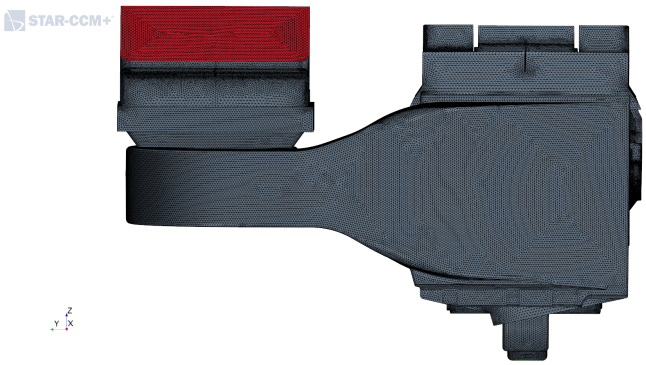

Fig. 2. Surface mesh schematic diagram.

Polyhedral meshes are adopted as the volume mesh type, which exhibit extremely high geometric adaptability and strong flexibility. The volume mesh was generated based on the surface mesh. A prism layer mesh was selected for the boundary layer, with a total thickness of 2 mm divided into 3 layers and a growth rate of 1.2. The maximum volume mesh size was set to 5 mm.

After determining the mesh type and the basic size, mesh independence verification was conducted to ensure the reliability of calculation results. The mass flow rate at the outlet and the far-field SPL were taken as evaluation criteria. Their values were compared at six kinds of meshes with different grid numbers as shown in Fig. 3.

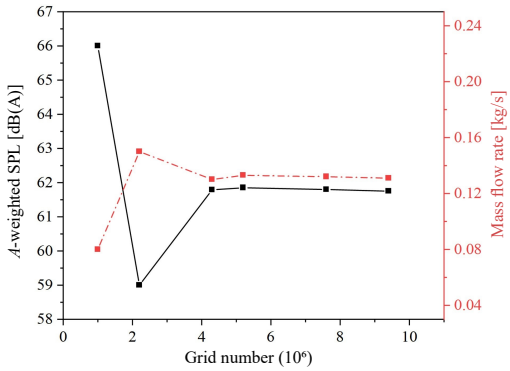

Fig. 3. Grid independence verification.

When the number of mesh elements increases from 4.23 million to 9.8 million, their difference of the flow rate at the outlets is less than 2 %, and the far-field SPL is less than 0.5 dB(A). Therefore, the final numerical calculation model adopts a mesh with 4.23 million elements, and the mesh generation result is shown in Fig. 4.

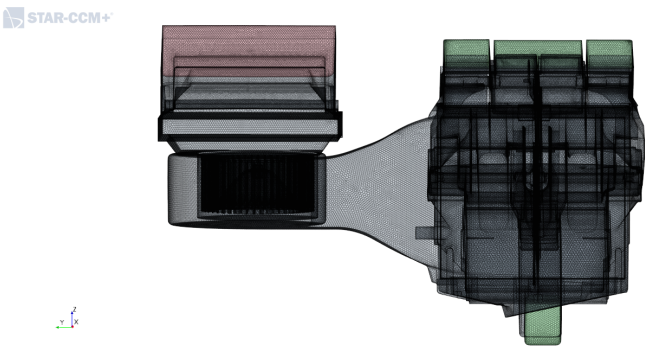

Fig. 4. Volume mesh schematic diagram.

2.4. Boundary conditions and solution

According to the actual operating conditions of the automotive vehicle air conditioning system, the inlet of the computational domain is set as a stagnation inlet, and the outlet is a pressure outlet. A no-slip wall condition is applied to accurately simulate the interaction between the fluid and the wall surfaces, including the development of the boundary layer and flow separation phenomena. The $y+$ wall treatment method is selected in this study. All settings are shown in Table 1.

Table 1. Steady-state calculation solver parameter settings.

Setting	Setting value
Temporal discretization scheme	Steady
Flow	Separated flow
Equation of state	Constant density
Reynolds-averaged turbulence	K-epsilon turbulent flow
K-epsilon turbulence models	Realizable k-ε two-layer model
Wall treatment method	Two-layer full $y+$ wall treatment
Rotating model	Moving reference frames
Acoustic model	Broadband noise source (BNS) model

For the internal flow field of the automotive air conditioning cabinet, the realizable k-ε model was selected as the physical model for the steady-state calculation. Based on the steady-state calculation, it is necessary to select an appropriate acoustic model to analyze the noise characteristics of the air conditioning system. This study adopts the broadband noise model, which is based on the Curle and Proudman equations for the solution. This model can effectively predict the distribution characteristics of broadband noise, providing a theoretical basis for subsequent noise optimization. The porosity of filter and evaporator was set to 0.8 according to the existing studies (Li, 2016; Zhang, 2019).

Transient calculation is performed after convergent steady-state calculation. In this study, the detached eddy simulation (DES) model is selected as the turbulence model for transient simulation. The rotating speed was set at 2266 rpm. Correspondingly, the transient calculation time step size was set at 7.3×10^{-5} s and the total simulation duration was 0.106 s. The FW-H acoustic method is adopted to obtain far-field aerodynamic noise of an air conditioning box under transient flow conditions. Far-field noise monitoring points are set at 1 m directly in front of the air conditioning cabinet air outlet (monitoring point A) and 1 m at a 45° diagonal direction (monitoring point B). The specific layout positions are shown in Fig. 5.

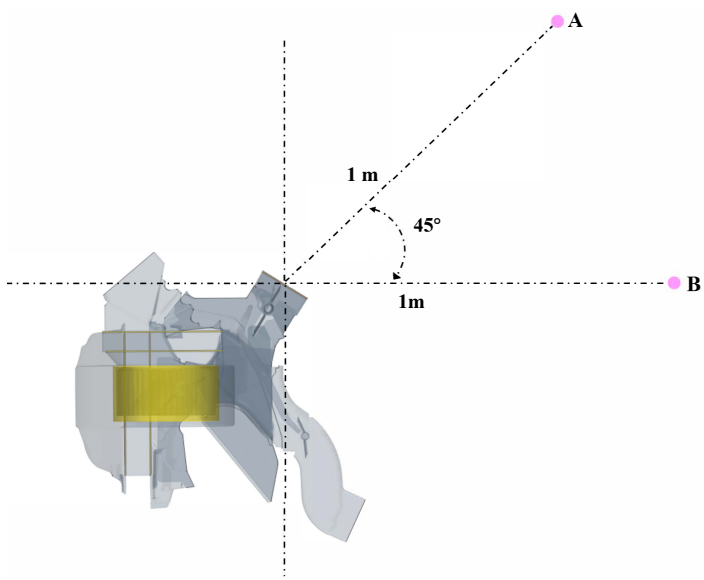

Fig. 5. Schematic diagram of far-field monitoring point locations.

2.5. Response surface methodology

The quadratic polynomial model is the most commonly used model for response surface experiments, and its general form is shown in Eq. (8):

$$Y = \beta_0 + \sum_{i=1}^{k} \beta_i X_i + \sum_{i=1}^{k} \beta_{ii} X_i^2 + \sum_{i<j} \beta_{ij} X_i X_j + \epsilon, \tag{8}$$

where Y is the response variable, X_i is the i-th independent variable (factor), β_0 is the constant term (intercept), β_i is the coefficient of the linear term, which determines the slope and direction of the response surface, β_{ii} is the coefficient of the quadratic term, representing the influence of the quadratic term of the i-th independent variable on the response variable, β_{ij} is the coefficient of the interaction term, which determines the distortion degree of the response surface and reflects the interaction between the independent variables, ϵ is the error term, which is usually assumed to follow a normal distribution, representing the random error unexplained by the model; the smaller the error term is, the stronger the predictive ability of the model is. The variance of the error term σ^2 is used to evaluate the uncertainty of the model, k is the number of independent variables.

For the convenience of calculation and analysis, the quadratic polynomial model can be expressed in matrix form as follows:

$$Y = \mathbf{X}\beta + \epsilon, \tag{9}$$

where Y is the vector of response variables, X is the design matrix containing the linear terms, quadratic terms and interaction terms of the independent variables, β is the vector of model coefficients, ϵ is the vector of error terms. Each row of the design matrix $\mathbf{X}$ corresponds to an experimental point, and each column corresponds to a model (e.g., linear, quadratic or interaction).

The model coefficients are usually estimated by the least squares method:

$$\widehat{\beta} = (X^{\mathrm{T}} X)^{-1} X^{\mathrm{T}} Y, \tag{10}$$

where $\widehat{\beta}$ is the estimated value of the model coefficients, X^{T} is the transpose of the design matrix, $(X^{\mathrm{T}} X)^{-1}$ is the inverse matrix of the design matrix. The objective of the least squares method is to minimize the sum of squared residuals, as shown in Eq. (11), where $\widehat{Y}_i$ is the predicted value of the model for the i-th experimental point:

$$\mathrm{SS}_{\mathrm{res}} = \sum_{i=1}^{k} (Y_i - \widehat{Y}_i)^2. \tag{11}$$

The coefficient of determination R^2 is used to evaluate the goodness of fit of the model:

$$R^2 = 1 - \frac{\mathrm{SS}_{\mathrm{res}}}{\mathrm{SS}_{\mathrm{tot}}}. \tag{12}$$

The adjusted coefficient of determination R^2_{adj} takes into account the number of model parameters:

$$R^2_{\mathrm{adj}} = 1 - \frac{\mathrm{SS}_{\mathrm{res}}/(n-p)}{\mathrm{SS}_{\mathrm{tot}}/(n-1)}, \tag{13}$$

where R^2 represents the proportion of the variation in the response variable explained by the model, R^2_{adj} takes into account the number of model parameters to prevent overfitting. Higher values of R^2 and R^2_{adj} indicate that the model has a good goodness of fit.

3. Aerodynamic noise characteristics

As shown in Fig. 6, the vehicle air conditioning simulation results indicate that dipole noise is mainly distributed on the surface of the fan blades and the outer area of the volute, with the maximum noise value at the

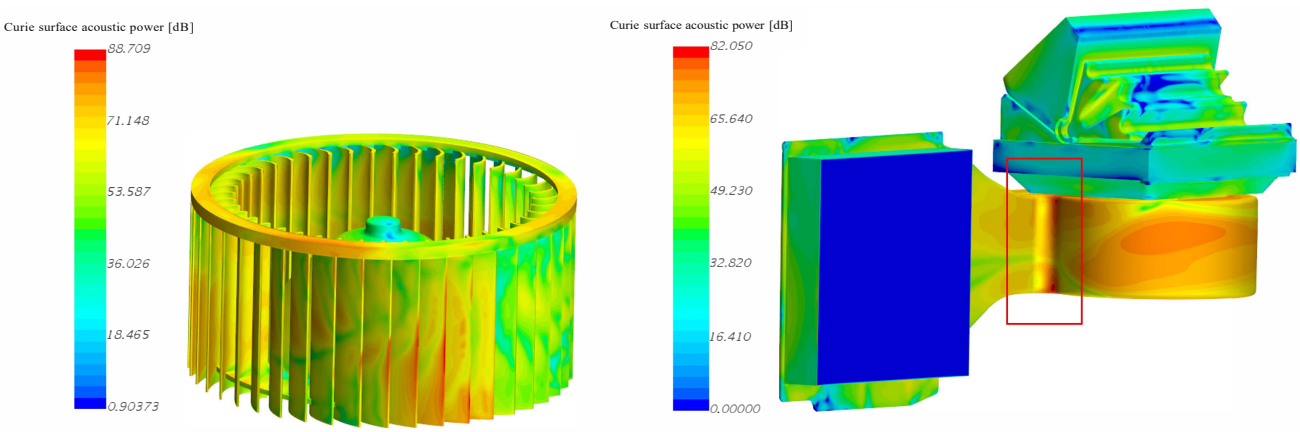

FIG. 6. Distribution of dipole noise on fan blades and volute under the operating condition of 2266 rpm.

blade edges reaching 88.7 dB. In addition, due to the small gap between the blades and the volute tongue, strong pressure fluctuations are likely to occur when air flows through. Consequently, the maximum dipole noise value at the volute consistently appears in the volute tongue area, with the maximum value being 82.0 dB.

To further analyze the contribution of different noise sources in the far-field SPL, the fan blades, the entire air conditioning system, and the air conditioning unit casing were respectively inputted as sound source. The SPL spectra are shown in Fig. 7. When the air conditioning unit casing is set as the noise source, the overall SPL spectrum is relatively low. And the noise intensity is higher in the low-frequency range around 500 Hz, which may be related to casing vibration or resonance of internal airflow. However, when the fan blades or the entire air conditioning system are used as the noise source, obvious peaks appear in the spectrum curve at the fundamental frequency and its harmonic frequencies. Due to the influence of the axial radiation characteristics of rotational noise, the peak amplitude at monitoring point A (directly facing the air outlet) is higher than that at monitoring point B (at a 45° diagonal angle).

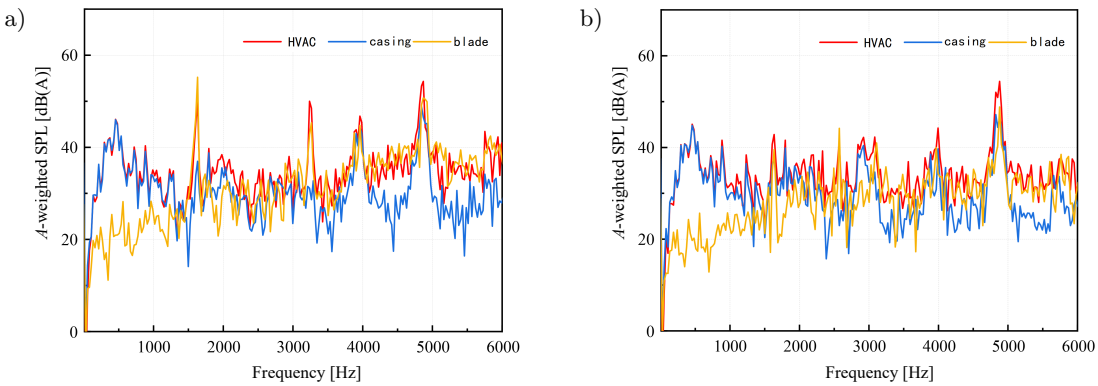

FIG. 7. Far-field SPL frequency spectrum curve: a) monitoring point A, b) monitoring point B.

After calculating the obtained sound pressure data, the total sound pressure levels of far-field noise are obtained, as shown in Table 2. When the entire air conditioning system and the fan are taken as noise sources, the far-

TABLE 2. Comparison of far-field total SPLs from different noise sources.

Noise source	Total SPL [dB(A)]
Entire vehicle air conditioning system	61.8
Casing	58.5
Fan blade	60.2

field SPLs reach 61.8 dB(A) and 60.2 dB(A), respectively. When the casing is regarded as the noise source, the total SPL is 58.5 dB(A). It could be found that the fan contributes more significantly to the far-field noise.

Based on the above analysis, the low noise optimization design would focus on the fan and its volute tongue part in subsequent work.

4. Noise reduction optimization based on RSM

According to the studies of former researchers (Wei *et al.*, 2023; Huang *et al.*, 2025; Bai *et al.*, 2024), the fan volute tongue gap (A), volute tongue radius (B), and blade outlet angle (C) were specifically selected as the variables for the designed experiment. Taking the far-field SPL (Y) of the automotive vehicle air conditioning system as the response, a full-factor experiment with 3 factors and 2 levels was designed. The levels of the experimental factors are shown in Table 3.

Table 3. Full factorial experimental factors and levels.

Factor levels	Volute tongue gap (A) [mm]	Volute tongue radius (B) [mm]	Blade outlet angle (C) [°]
1	8	10	110
2	12	16	150

In this study, the central composite design (CCD) method was selected for the design of the RSM experiment. The specific experimental design and the corresponding result are shown in Table 4.

Table 4. Response surface experimental design table and results.

Run order	Point type	Volute tongue gap (A) [mm]	Volute tongue radius (B) [mm]	Blade outlet angle (C) [°]	Far-field SPL (Y) [dB(A)]
1	1	8	10	110	58.7
2	1	12	10	110	57.0
3	1	8	16	110	59.4
4	1	12	16	110	58.1
5	1	8	10	150	61.1
6	1	12	10	150	60.8
7	1	8	16	150	62.1
8	1	10	16	150	63.0
9	−1	10	13	130	57.8
10	−1	10	13	130	58.3
11	−1	10	13	130	58.0
12	−1	10	13	130	58.3
13	−1	10	13	130	58.1
14	−1	10	13	130	58.4
15	0	6.63	13	130	58.7
16	0	13.36	13	130	57.8
17	0	10	7.9546	130	59.9
18	0	10	18.0454	130	62.3
19	0	10	13	96.36	57.9
20	0	10	13	163.6	64.2

Analysis of variance (ANOVA) is performed on the designed experimental results, as shown in Table 5. It can be seen from the ANOVA table that the model is significant ($P < 0.05$) and there is no significant LOF ($P > 0.05$), except for the quadratic term AA (volute tongue gap × volute tongue gap). This indicates that the model includes all significant terms, while the term AA is insignificant. Next, it is necessary to evaluate the model fitting performance by examining the coefficient of determination (R^2) and the adjusted coefficient of determination (R^2_{adj}). The results are shown in Table 6.

Table 5. Analysis of variance (ANOVA).

Source	Degree of freedom (DOF)	Adjusted sum of squares	Adjusted mean squares	F-value	P-value
Model	9	78.2561	8.6951	137.40	0.001
Linear	3	50.0515	16.6838	263.64	0.001
Volute tongue gap (A)	1	1.0632	1.0632	16.80	0.002
Volute tongue radius (B)	1	5.8159	5.8159	91.90	0.008
Blade outlet angle (C)	1	43.1724	43.1724	682.20	0.015
Quadratic	3	26.0821	8.6940	137.38	0.005
A^2	1	0.0006	0.0006	0.01	0.922
B^2	1	14.1351	14.1351	223.36	0.00
C^2	1	13.9841	13.9841	220.97	0.000
Two-factor interaction (TFI)	3	2.1226	0.7075	11.18	0.002
AB	1	0.3200	0.3200	5.06	0.048
AC	1	1.5138	1.5138	23.92	0.001
BC	1	0.2888	0.2888	4.56	0.058
Error	10	0.6328	0.0633	–	–
Lack of fit (LOF)	5	0.3887	0.0777	1.59	0.311
Pure error (PE)	5	0.2441	0.0488	–	–
Total	19	78.8890	–	–	–

Table 6. Model summary.

R^2	R^2_{adj}
0.992	0.9848

It can be seen from Table 6 that the coefficient of determination (R^2) for the overall fitting performance and the correlation factor (R^2_{adj}) are both higher than 0.95, indicating that the model exhibits excellent fitting and predictive performance.

Since the quadratic term AA (volute tongue gap × volute tongue gap) in the model is insignificant, and no abnormalities were observed in the model residuals, only the AA term was removed for model refinement and refitting. As shown in Table 7, the adjusted coefficient of determination (R^2_{adj}) increased by 0.13 %, respectively, compared with the original model. It indicates that the model's fitting performance has been improved after eliminating the insignificant term, and it exhibits enhanced predictive capability. After removing the insignificant term, the regression equation for the response value Y (far-field SPL) is obtained as follows:

$$Y = 129.22 - 1.987A - 3.39B - 0.7017C + 0.11011B^2 + 0.002464C^2 + 0.0333AB + 0.01087AC + 0.00317BC. \quad (14)$$

Table 7. Comparative model summary: original vs. reduced model.

	Original model	Processed model	Change
R^2	0.992	0.992	–
R^2_{adj}	0.9848	0.9861	↑

Based on the fitted regression equation, response surface plots were generated to analyze the effects of factors A (volute tongue gap), B (volute tongue radius), and C (blade outlet angle) on the response Y (far-field SPL). The results are shown in Fig. 8.

It can be observed from Fig. 8a that when the blade outlet angle is kept constant at 130°, the far-field SPL decreases with the increase of the volute tongue gap. As the volute tongue radius increases, the far-field SPL first decreases and then increases, indicating that there exists a minimum value within the selected factor level range. This indicates that the effect of the volute tongue radius in the far-field SPL is not a linear relationship. It can be seen from Fig. 8b that when the volute tongue radius is maintained at 13 mm, the far-field SPL first decreases and then increases as the blade outlet angle increases. It can also be observed from Fig. 8c that the response

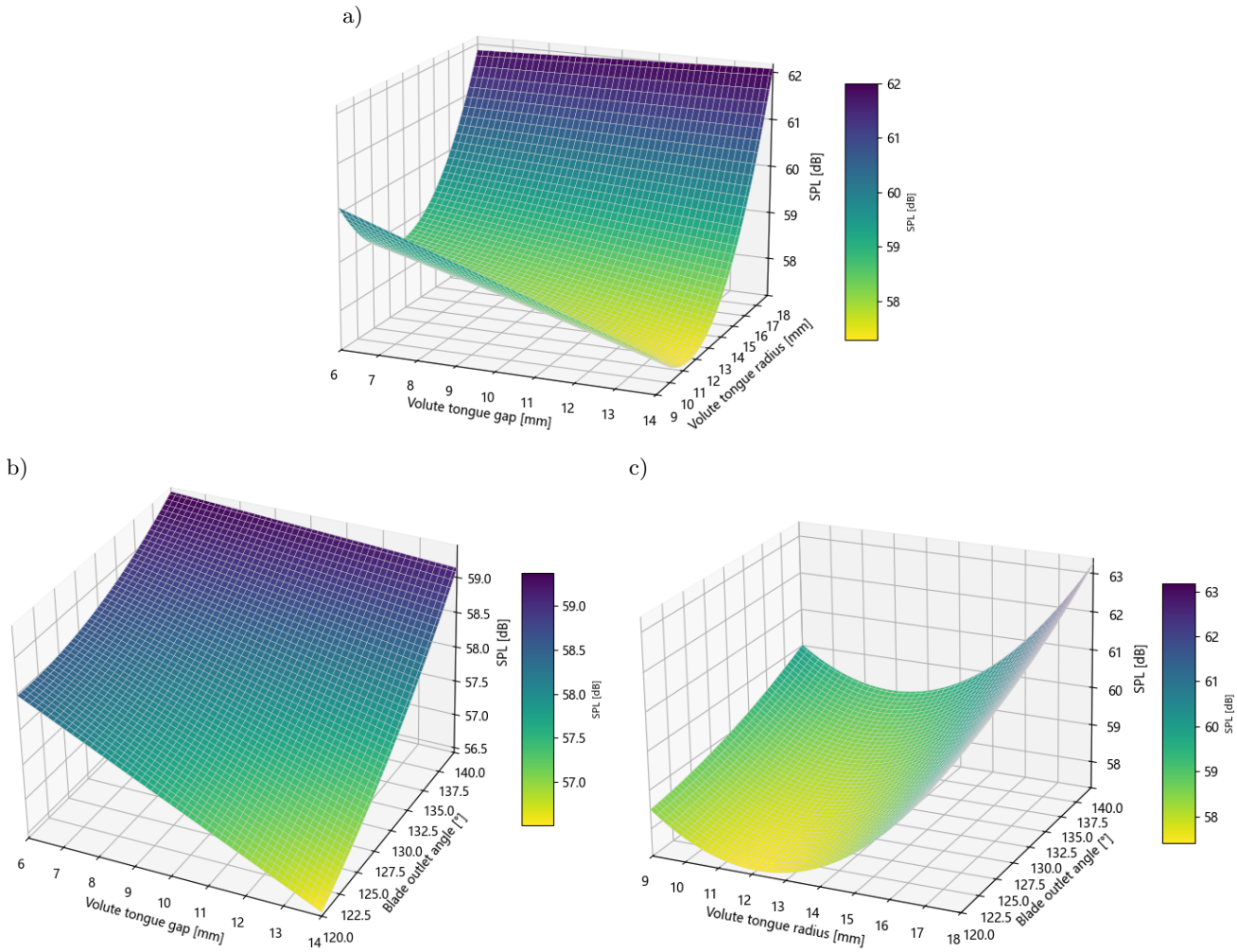

Fig. 8. Far-field SPL response surface plot: a) A vs. B, b) A vs. C, c) B vs. C.

surface plot exhibits a curved surface, confirming that the minimum value of the far-field SPL exists within the selected factor level range.

After the response surface test, the response optimizer function in Minitab software can be used to calculate the predicted values and confidence intervals of the model under optimal conditions. The response optimizer is employed to predict the optimal conditions for the model, and the factor combination corresponding to the minimum value of the response Y (far-field SPL) is determined, as detailed in Table 8.

Table 8. Response optimization solution.

Volute tongue gap (A) [mm]	Volute tongue radius (B) [mm]	Blade outlet angle (C) [°]
13.36	11.83	110

Simulation verification was performed on the factor combination of the optimal solution obtained by Minitab software, and a comparison was conducted with the original model data. The results are shown in Table 9. The total SPL at the far-field monitoring point was reduced by 6.3 dB(A), indicating a significant optimization effect.

Table 9. Comparative analysis: optimized vs. original model.

Scheme	Far-field SPL [dB(A)]
Original structure	61.8
Optimized structure	55.5

5. Conclusion

A reliable vehicle air conditioning system simulation model was established, in which non-critical structures were simplified. Filters/evaporators were treated as porous media (porosity = 0.8). Triangular surface meshes, polyhedral volume meshes with local densification and 3-layer prism boundary meshes were adopted. Grid-independence verification ensured reliability. Steady-state simulations used realizable k-ε and BNS models; transient simulations adopted DES and FW-H methods (time step = 7.3×10^{-5} s) to capture flow and acoustic characteristics.

Dipole noise mainly distributed on the fan blades (max 88.7 dB) and volute tongue (max 82.0 dB) due to pressure fluctuations. Different sound sources contribute differently to far-field noise. When the air conditioning unit casing is inputted as the noise source, the far-field SPL is 58.5 dB(A) and noise intensity is higher in the low-frequency range around 500 Hz. When the fan blades and the entire system is used as the noise source, the far-field SPL reaches 60.2 dB(A) and 61.8 dB(A), respectively, and obvious peaks appear in the spectrum curve at the fundamental frequency and its harmonic frequencies.

With volute tongue gap (A), radius (B), and blade outlet angle (C) as variables, and SPL as the response, a CCD experiment was conducted for RSM. An insignificant term was removed, and ANOVA confirmed the quadratic model's significance ($P < 0.05$) and good fitting ($R^2 = 0.992$, $R^2_{\text{adj}} = 0.9861$). The model exhibits excellent fitting and predictive performance. The regression equation for the response value was obtained, and the optimal parameter combination ($A = 13.36$ mm, $B = 11.83$ mm, $C = 110°$) reduced SPL from 61.8 dB(A) to 55.5 dB(A).

Fundings

This work was supported by Xiezhong International Thermal Management Systems (Jiangsu) Co., LTD. (contract no. 2024321103000540).

Conflict of interests

The authors declare that there are no known competing financial interests or personal relationships that could have influenced the work described in this paper.

Authors' contributions

Cheng Qian performed simulation, and wrote the manuscript, Dajian Wang and Hao Wang established the model and determined main parameters. Fushen Tang conducted data collection and data analysis. Min Lin performed simulation and made the plots. Jinjin Xu checked and optimized the manuscript and guided the whole study process. All authors reviewed and approved the final manuscript.

References

1. Aissaoui A. *et al.* (2015), Flow-induced noise optimization of SUV HVAC system using a lattice Boltzmann method, *SAE International Journal of Passenger Cars – Mechanical Systems*, **8**(3): 1053–1062, https://doi.org/10.4271/2015-01-2323.

2. Bai M., Liu Z., Ling Y., Tan H. (2024), Effect of impeller structure on aerodynamic performance and noise reduction of a small multi-blade centrifugal fan, *Science and Technology for the Built Environment*, **30**(6): 563–578, https://doi.org/10.1080/23744731.2024.2357526.

3. Guo R., Mi T., Li L., Luo R. (2022), Research on aerodynamic performance and noise reduction of high-voltage fans on fuel cell vehicles, *Applied Acoustics*, **186**: 108454, https://doi.org/10.1016/j.apacoust.2021.108454.

4. Heo S., Cheong C., Kim T.-H. (2011), Development of low-noise centrifugal fans for a refrigerator using inclined S-shaped trailing edge, *International Journal of Refrigeration*, **34**(8): 2076–2091, https://doi.org/10.1016/j.ijrefrig.2011.07.003.

5. Huang Y., Zhang H., Liu Z. (2025), Realizable k-ε model-based gradual-radius volute tongue on aerodynamic performance and noise of multi-wing centrifugal fan, *Applied Sciences*, **15**(17): 9471, https://doi.org/10.3390/app15179471.

6. Lee C., Kil H.-G. (2010), An aero-acoustic performance prediction method of Sirocco fan, [in:] *Proceedings of the ASME 2010 3rd Joint US-European Fluids Engineering Summer Meeting collocated with 8th International Conference on Nanochannels, Microchannels, and Minichannels. ASME 2010 3rd Joint US-European Fluids Engineering Summer Meeting*, pp. 813–817, https://doi.org/10.1115/FEDSM-ICNMM2010-31040.

7. Lee D., Perot F., Ih K.-D., Freed D. (2011), Prediction of flow-induced noise of automotive HVAC systems, *SAE 2011 World Congress & Exhibition*, https://doi.org/10.4271/2011-01-0493.

8. Li S. (2016), *Flow noise analysis of Class A automotive HVAC systems* [in Chinese], MA Thesis, *Jilin University*.

9. Liu S., Li S. (2022), A brief discussion on the hazards and sources of automobile noise [in Chinese], *Times Automobile*, (4): 29–31.

10. Moreau D.J., Doolan C.J. (2016), The generation of tonal noise from sawtooth trailing-edge serrations at low Reynolds numbers, *The Aeronautical Journal*, **120**(1228): 971–983, https://doi.org/10.1017/aer.2016.39.

11. Ravichandran A., Logdesser A., Peller N., Manhart M. (2023), Acoustic resonances in an automotive HVAC outlet, *Journal of Sound and Vibration*, **569**: 118051, https://doi.org/10.1016/j.jsv.2023.118051.

12. Sevant N.E., Bloor M.I.G., Wilson M.J. (2000), Aerodynamic design of a flying wing using response surface methodology, *Journal of Aircraft*, **37**(4): 562–571, https://doi.org/10.2514/2.2665.

13. Singh S., Mohanty A.R. (2018), HVAC noise control using natural materials to improve vehicle interior sound quality, *Applied Acoustics*, **140**: 100–109, https://doi.org/10.1016/j.apacoust.2018.05.013.

14. Wei Y., Li L., Lun Y., Wang Z., Yang H., Zhang W. (2023), Effect of volute-tongue clearance on the aerodynamic performance and noise of multi-wing centrifugal fan for air conditioning, *Journal of Applied Fluid Mechanics*, **16**(7): 1483–1498, https://doi.org/10.47176/jafm.16.07.1514.

15. Wu Z., Zhou S., Li Y., Jin W., Luo Y. (2023), Air duct optimization design based on local turbulence loss analysis and IMOCS algorithm, *Machines*, **11**(2): 129, https://doi.org/10.3390/machines11020129.

16. Yang Z., Gu Z., Wang Y., Yan J., Yang X. (2013), Prediction and optimization of aerodynamic noise in an automotive air conditioning centrifugal fan, *Journal of Central South University*, **20**(5): 1245–1253, https://doi.org/10.1007/s11771-013-1608-6.

17. Zhang C., Li A., Li J., Hou Y., Chen X. (2021), Radiation noise control of a 90° rectangular elbow in ventilation and air conditioning systems, *Journal of Building Engineering*, **37**: 102157, https://doi.org/10.1016/j.jobe.2021.102157.

18. Zhang F. (2019), Analysis of aerodynamic noise transfer characteristics and noise reduction optimization of automotive air conditioning blowers [in Chinese], MA Thesis, *Southwest Jiaotong University*.

19. Zhang L., Wu K., Liu Y. (2017), Investigation on multi-objective performance optimization algorithm application of fan based on response surface method and entropy method, *Journal of Thermal Science*, **26**(6): 533–539, https://doi.org/10.1007/s11630-017-0970-3.